SCIENCE CHINA
Chemistry

•ARTICLES•

https://doi.org/10.1007/s11426-018-9282-4

Enzyme responsive supramolecular hydrogels assembled from nonionic peptide amphiphiles

Rui Liu, Zhekun Shi, Jing Sun* & Zhibo Li*

Key Laboratory of Biobased Polymer Materials, Shandong Provincial Education Department; School of Polymer Science and Engineering, Qingdao University of Science and Technology, Qingdao 266042, China

Received March 22, 2018; accepted May 15, 2018; published online August 2, 2018

Smart peptide hydrogels are of great interest for their great potential applications. Here, we report a facile approach to prepare a class of enzyme-responsive hydrogels in a scalable manner. These hydrogels self-assemble from a family of nonionic peptide amphiphiles (PAs) synthesized by sequential ring-opening polymerization (ROP) of γ-benzyl-*L*-glutamate *N*-carboxyanhydride (BLG-NCA) and *L*-tyrosine *N*-carboxyanhydride (Tyr-NCA), followed by subsequent aminolysis. These PA samples can readily form a clear hydrogel with a critical gelation concentration as low as 0.5 wt%. The incorporation of tyrosine residues offers hydrophobicity, hydrogen-bonding interaction and enzyme-responsive properties. The hydrogel-to-nanogel transition is observed under physiological conditions in the presence of horseradish peroxidase (HRP) and hydrogen peroxide (H_2O_2). The obtained PA hydrogels are ideal candidates for the new generation of smart scaffolds.

oligopeptides, ring-opening polymerization, hydrogel, nanogel, enzyme responsive

Citation: Liu R, Shi Z, Sun J, Li Z. Enzyme responsive supramolecular hydrogels assembled from nonionic peptide amphiphiles. *Sci China Chem*, 2018, 61, https://doi.org/10.1007/s11426-018-9282-4

1 Introduction

Peptide based hydrogel offers great potential for biomedical applications such as drug delivery carrier [1,2] and 3D scaffold [3–6] due to its good biocompatibility and versatile biofunctionalization [7–9]. Peptide hydrogel can be easily obtained from both natural peptides [10] and synthesized peptide amphiphiles (PAs) [11–13]. In contrast to the natural peptide hydrogels with certain limitations in heterogeneity and sources, the synthetic peptide hydrogels based on PAs offer more advantages in versatility, functionality, stability and processability. Stupp and coworkers [14–16] have systematically studied a series of PAs hydrogels from sequence-specific oligopeptides by solid-phase synthesis. Despite the great progress made in PA hydrogels, they generally contain charged amino acid residues, which may cause inevitable protein absorption *in vitro*. Further, the production in large scale and practical applications still remain a great challenge. To tackle this problem, our group [17,18] developed a robust, convenient and easily scalable approach by post-modification of well-defined alkyl-oligopeptide precursors to prepare nonionic PAs, which offer great opportunities to expand the versatility of PA hydrogels.

Lately, stimuli-responsive hydrogels, referred as smart hydrogels that can rapidly respond in a controlled manner to the external stimuli have received great interest [19,20]. Horseradish peroxidase (HRP) is an enzyme with good biocompatibility, which is generally used for triggering the intermolecular cross-linking via catalyzing the radical coupling of aniline and phenol moieties in the presence of hydrogen peroxide. It has been reported that HRP and H_2O_2 can facilitate the hydrogelation of polysaccharide hydrogels [21,22]. Recently, a few research groups have reported the polymers modified with the tyrosine residues on the side

*Corresponding authors (email: jingsun@qust.edu.cn; zbli@qust.edu.cn)

chain can form hydrogels or colloidal particles by adding HRP and H_2O_2 [23–27].

Herein, we prepared a novel class of nonionic peptide amphiphile (PA) by sequential ring-opening polymerization (ROP) of γ-benzyl-*L*-glutamate *N*-carboxyanhydride (BLG-NCA) and *L*-tyrosine *N*-carboxyanhydride (Tyr-NCA) using hexamethyldisilazane (HMDS) as an initiator, followed by aminolysis with ethanolamine. These PA samples can readily form a clear hydrogel with a critical gelation concentration as low as 0.5 wt%. The hydrogel-to-nanogel transition is observed under physiological conditions in the presence of horseradish peroxidase (HRP) and hydrogen peroxide (H_2O_2).

2 Experimental

2.1 Materials and methods

Hexane and tetrahydrofuran (THF) were purified by passing through activated alumina columns prior to use. HRP, hexamethyldisilazane (HMDS, 99%) and ethanolamine (EA) were purchased from Aladdin (USA). Hydrogen peroxide (H_2O_2), diethyl ether and 2-hydroxypyridine (2-HP) were purchased from Sinopharm Chemical Reagent Co., Ltd. (China). *N*,*N*-Dimethylformamide (DMF) was stored over calcium hydride (CaH_2) and purified by vacuum distillation with CaH_2. Benzyl-*L*-glutamic acid and *L*-Tyrosine acid were purchased from GL Biochem (China) Ltd.

2.2 Synthesis of γ-benzyl-*L*-glutamate *N*-carboxyanhydride (BLG-NCA) and *L*-tyrosine *N*-carboxyanhydride (Tyr-NCA)

γ-Benzyl-*L*-glutamate BLG (20 g, 84.3 mmol) was suspended in anhydrous THF (200 mL) at 50 °C and stirred under N_2. Triphosgene (8.88 g, 30 mmol) was then added. After the reaction solution became clear, the reaction solution was cooled and then precipitated in *n*-hexane (500 mL). The mixture was filtered and recrystallization in THF/hexane. 14.6 g BLG-NCA was obtained. Yield: 68.7%. Tyr-NCA was synthesized by reacting *L*-tyrosine with triphosgene in dry THF in N_2 atmosphere in a similar way. Yield: 76.4%.

2.3 Synthesis of oligo(γ-benzyl-*L*-glutamate)-*b*-oligo(*L*-tyrosine) (BLG-*b*-Tyr) oligomers

BLG-NCA was dissolved in 40 mL dry DMF in a reaction flask, followed by addition of HMDS in DMF solution at room temperature. The polymerization was monitored by observing the disappearance of characteristic peaks from NCA (1790 and 1850 cm^{-1}) using an FTIR spectrometer at room temperature. After the peaks disappeared, the Tyr-NCA monomer was added into the solution. After complete reaction, the solution was precipitated in excess amount of cold diethyl ether (67.3% yield). The obtained product was further washed twice with diethyl ether and dry overnight under vacuum.

2.4 Aminolysis of BLG-*b*-Tyr oligomers

The BLG-*b*-Tyr oligomer and ethanolamine (EA) (8 equivalent of the benzyloxycarbonyl groups) were dissolved in dry DMF in a reaction flask with agitator, then 2-hydroxypyridine (2-HP) (5 equivalent of the benzyloxycarbonyl units) was added to as a catalyst. The aminolysis reaction proceeded under a N_2 atmosphere at 50 °C for 48 h. After that, most of the solution DMF was removed using rotary evaporator to give a crude concentrated product solution. The crude product was precipitated in excess diethyl ether. By re-dissolving the product into deionized water and dialysis (1000 Da molecular weight cutoff) against deionized water for 48 h, the light yellow spongy powder oligo(*L*-glutamate-*g*-EA)-*b*-oligo(*L*-tyrosine) (G-EA)-*b*-Tyr oligomers was obtained after lyophilization (58.5% yield).

2.5 Preparation of hydrogel

Hydrogel solutions were prepared by dissolving freeze-dried the oligopeptide samples in deionized water at the desired concentrations. The homogeneous solutions were obtained by sonication and blow heating. The formation of the gel was determined via inverting tube method.

2.6 Enzymatic reaction

All samples were prepared in vials by enzymatic oxidation using HRP and H_2O_2 at room temperature. In a typical procedure, $(G\text{-}EA)_4\text{-}Tyr_2$ was dissolved in phosphate buffered solution (PBS, pH 7.4), freshly prepared PBS solution of HRP (30 U mL^{-1} stock solution) and H_2O_2 were added and the mixture was gently vortexed, followed by standing overnight at room temperature. In all cases, the mole ratio of H_2O_2 to the phenol group was fixed at 0.5 and the final concentration is 1 wt%. The experiments for $(G\text{-}EA)_6\text{-}Tyr_3$ and $(G\text{-}EA)_8\text{-}Tyr_4$ were performed in a similar way.

2.7 Characterizations

^1H NMR spectra were recorded on Bruker AV500 FT-NMR spectrometer (Germany). FTIR spectra were performed by using a Bruker HQL005 FTIR spectrometer (Germany) by using the transmission method (TR). MALDI-TOF mass spectrometry analysis was performed on a Bruker Microflex-LRF mass spectrometer. TEM experiments were conducted on FEI TECNAI 20 (USA). 3 mL of the oligopeptide solu-

tion at a concentration of 0.5% was pipetted onto the carbon-coated copper grid, which was pretreated in a plasma cleaner. The grid was blotted to remove any excess solution and then dyed using 0.2% uranyl acetate. The samples were dried and stored under ambient conditions before TEM testing. For SEM experiment, the products need to be freeze-dried at gel to get loose solid, then take a little sample directly on the conductive adhesive of the sample table. SEM measurements were carried on a JEOL JSM-7500F instrument (Japan). The dilute micelle solution was deposited on a silicon wafer to a very thin layer and dried at room temperature. A thin layer of Au was coated on the sample surface before measurement. AFM studies were conducted using tapping mode AFM under ambient conditions. 3 mL of oligopeptide solution at a concentration of 0.5 wt% was placed on freshly cleaved mica, and then the samples were dried and stored under ambient conditions before AFM testing. The rheological properties of hydrogels were measured on a torque rheometer (TA) modular rheometer operating in a plate mode (diameter: 40 mm) at 25 °C. A dynamic strain sweep (from 0.1% to 200% strain, 1 Hz oscillation) was conducted. The size of nanostructure was evaluated by using dynamic light scattering (DLS, NANO ZS90 from Malvern Instruments, UK) before and after adding enzymes.

3 Results and discussion

The γ-benzyl-*L*-glutamate *N*-carboxyanhydride (BLG-NCA) and *L*-tyrosine *N*-carboxyanhydride (Tyr-NCA) monomers were synthesized following the reported methods [19,28,29]. The chemical structures of BLG-NCA and Tyr-NCA were confirmed by ^{1}H NMR spectroscopy (Figures S1 and S2, Supporting Information online). The block oligopeptides were synthesized by sequential ROP of BLG-NCA and Tyr-NCA using HMDS as the initiator (Scheme S1, Supporting Information online). FTIR was used to monitor the conversion of NCA monomers to oligopeptides. As the characteristic peaks of the first BLG-NCA disappeared, the Try-NCA monomer was then added. All peaks of the synthesized oligo (γ-benzyl-*L*-glutamate)-*b*-oligo(*L*-tyrosine) (BLG-*b*-Tyr) oligopeptides are well assigned in the ^{1}H NMR spectra, which confirm the chemical structures (Figure 1(a)). A series of oligopeptides with different degrees of polymerization (DPs) have been successfully prepared by varying the amine initiator/NCAs ratio. The oligo(*L*-glutamate-*g*-EA)-*b*-oligo (*L*-tyrosine) (G-EA)-*b*-Tyr PA samples were obtained by direct aminolysis of the benzyl ester group with ethanolamine (EA), which is highly efficient in high yields under mild reaction condition [17,18,30]. The modification of oligopeptides was verified by ^{1}H NMR spectroscopy (Figure 1(b)). All the peaks are well assigned and benzyl ester bonds are completely converted into amide bonds as indicated by disappearance of the peaks at 7.36 and 5.20 ppm. The molecular structures and average molecular weights were further characterized by matrix-assisted laser desorption ionization (MALDI) mass spectrometry (Figures S3–S7). The molecular characteristics of all molecules are given along with their abbreviations in Table 1.

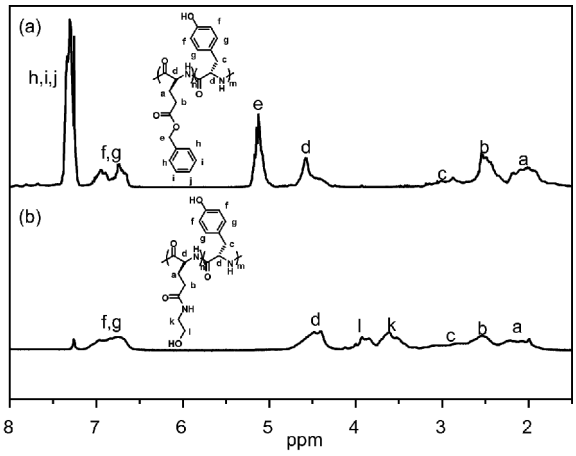

Figure 1 ^{1}H NMR spectra of (a) BLG_4-*b*-Tyr_2 and (b) $(G\text{-}EA)_4$-*b*-Tyr_2 in a mixture of $CDCl_3/CF_3COOD$ (*v*/*v*=10:1).

Most of the PA samples can be easily dispersed in the deionized water and form self-supported hydrogels at a concentration as low as 0.5 wt%. A typical photo of a clear hydrogel formed from a $(G\text{-}EA)_4$-*b*-Tyr_2 sample at a concentration of 0.5 wt% is shown in Scheme 1. The critical gelation concentration (CGC) is determined by an inverting tube method (Table 1). It is observed that the increase of the degree of polymerization (DP) can lead to the increasing CGC, indicating the reduced gelation property. It is generally accepted that the chain length of the polypeptides can largely influence the secondary structure, for example oligopeptides with longer chain length tend to form stable *α*-helix structure [31,32]. The influence of chain length on secondary structure of the oligopeptides was thus studied. The attempt to use CD

Table 1 The molecular characteristics of the nonionic oligopeptide amphiphilies

Sample	$(G\text{-}EA)_4$-*b*-Tyr_2	$(G\text{-}EA)_6$-*b*-Tyr_1	$(G\text{-}EA)_6$-*b*-Tyr_3	$(G\text{-}EA)_6$-*b*-Tyr_5	$(G\text{-}EA)_8$-*b*-Tyr_4
Feed ratio ($I/M_1/M_2$)	1/4/2	1/6/1	1/6/4	1/6/6	1/9/5
DP(n/m)[a)]	4/2	6/1	6/3	6/5	8/4
CGC[b)]	0.5%	Sol	0.9%	Precipitate	1.8%

a) Calculated from ^{1}H NMR spectra and MAIDI-TOF MS. b) Determined by inverting tube method.

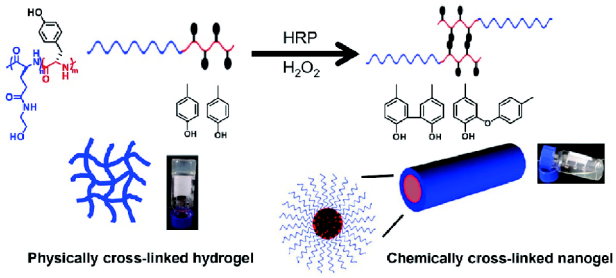

Scheme 1 The transition from physically cross-linked hydrogel to chemically cross-linked nanogel by the addition of enzyme (color online).

spectroscopy to investigate the secondary structure failed due to the weak signals. We thus performed FTIR measurements to characterize the samples. The FTIR spectra of $(G\text{-}EA)_4$-*b*-Tyr_2 oligomers are shown in Figure 2. It can be seen that the absorption peaks of the sample locate at 1628 and 1520 cm^{-1} with broad shoulders at higher wavenumber, indicating the dominant β-sheet conformation [33]. This is expected as both oligo(G-EA) and oligoTyr are reported to adopt the β-sheet conformation [34]. We further studied the gelation behavior as a function of chain length of PAs at a fixed molar ratio of G-EA to Tyr of 2:1. As the entire chain length increases, the main adsorption peaks shift to 1647 and 1545 cm^{-1} with broad shoulders. This suggests that the oligo (G-EA) segments have more content of intramolecular interactions, and probably adopt partial and dynamic *α*-helix conformation [19]. We thus assume that transformation of intermolecular hydrogen bonding among PA molecules to partial intramolecular interactions can reduce the gelation ability and consequently increase the CGCs of PA samples. The reason is that decrease of intermolecular hydrogen bonding can seriously reduce the long range ordering within the assemblies. We investigated the effect of molar ratio of G-EA to Tyr on the gelation behavior of PAs with constant DP of G-EA segment. It is observed that increasing the chain length of oligo(*L*-tyrosine) to 5 can result in the precipitation from aqueous solution. This is possibly due to the enhanced hydrophobicity and intermolecular hydrogen bonding of the system. Both can result in the aggregation of the oligo(*L*-tyrosine)s. As the DP of oligo(*L*-tyrosine) decreases to 1, the oligomer remains sol state over the entire experimental window, suggesting the good solubility. All these results indicate that the hydrophilic-hydrophobic balance and hydrogen bonding is crucial for the self-assembly and gelation ability [18].

We performed SEM to characterize the detailed structure of the oligopeptide hydrogels. Figure 3(a) shows the typical morphology of 3D network of the hydrogel of sample $(G\text{-}EA)_4$-*b*-Tyr_2. TEM was further employed to study the detailed nanostructure of the hydrogels. It is observed that $(G\text{-}EA)_4$-*b*-Tyr_2 self-assembles into ultralong 1D fiber-like structures with a length of more than 1 μm and a diameter of

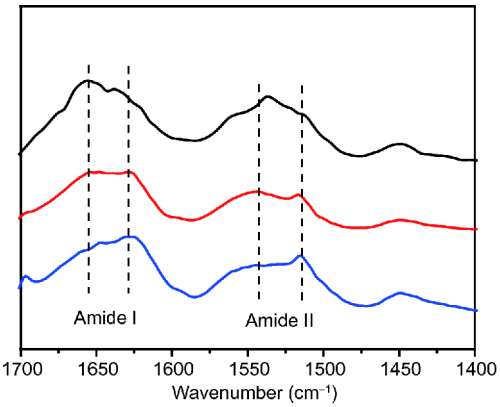

Figure 2 The solid-FTIR spectra of $(G\text{-}EA)_4$-*b*-Tyr_2 (blue line), $(G\text{-}EA)_6$-*b*-Tyr_3 (red line), $(G\text{-}EA)_8$-*b*-Tyr_4 (black line) samples (color online).

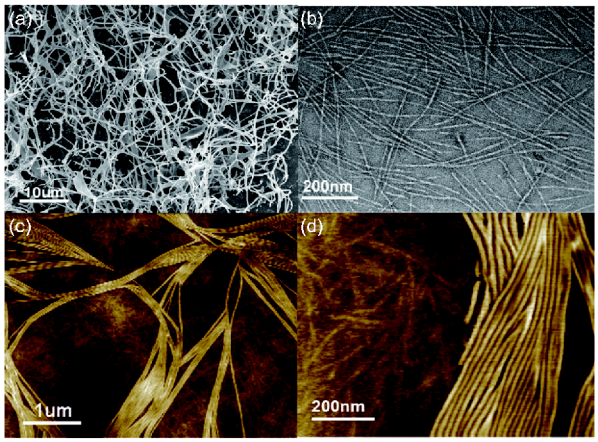

Figure 3 (a) SEM image of freeze-dried $(G\text{-}EA)_4$-*b*-Tyr_2 gel. (b) TEM and (c, d) AFM images of $(G\text{-}EA)_4$-*b*-Tyr_2 at a concentration of 0.5 wt% (color online).

6~9 nm, as shown in Figure 3(b). AFM confirms the formation of nanofibers and the diameter (6~8 nm) is consistent with that from TEM measurement (Figure 3(c, d)). Note that the height is observed to be ~7 nm, comparable to the diameter. This suggests that PA samples form the cylindrical structure instead of planar ribbon. In addition to the individual fiber, nanoribbons or nanobelts with similar height of ~7 nm are also observed. We presume that these planar structures are formed by several of protofilaments adhesive to each other through the hydrogen bonding between the hydroxyl groups, as indicated in Figure 3(d) [16]. It is known that PA molecule containing a hydrophobic alkyl chain segment and a hydrophilic peptide block can self-assemble into a 1D nanofibers, driven by both collapse of hydrophobic alkyl tails and hydrogen bonding between β-sheets of peptides blocks [15,33]. Similarly, we propose a possible mechanism of hydrogel formation. The nanofiber forms with hydrophobic oligoTyr as the core and hydrophilic oligo(G-EA) as the comprising outer the surface. It is driven by hydrophilic-hydrophobic interaction and hydrogen bonding, which further results in the 3D hydrogel network [18]. Note

that in addition to π-π interactions and hydrophobicity involving by the aromatic side chains, tyrosine residues offer complementary hydrogen-bonding interactions from the tyrosine −OH group that generally favors the protein stability [34,35]. Similarly, both other samples also exhibit fiber-like structures with diameters of 7–10 nm and 8–12 nm, respectively (Figure S8**)**. It is evident that the higher DP increases the diameter of the nanofibers, consistent with the model we proposed.

The mechanical properties of the hydrogels were investigated by rheology measurement. We show a dynamic strain sweep for the hydrogel from (G-EA)$_4$-*b*-Tyr$_2$ oligomer (3.5 wt%) in the strain range of 0.1%–200% with ω=6 rad s^{-1} at room temperature (Figure S9). The storage modulus (G') is ~656 Pa, which is approximately one order of magnitude larger than the loss modulus (G''), indicative of the solid gel state (Figure 4). As expected, the G' increases as DP of oligomers decreases, confirming the enhanced gelation ability. This is consistent with the previous results. Further, G' increases with an increase in concentration of the PAs, indicative of strong hydrogels. This is due to the increased physical crosslinking (entanglement point) as a result of increased numbers of fibrils [18].

As previously reported, the presence of H_2O_2 and HRP in the system can lead to chemical cross-linking of phenolic hydroxyl groups [25,26,36–39]. Interestingly, an unusual gel-to-sol transition is observed for (G-AE)$_4$-*b*-Tyr$_2$ hydrogel upon adding enzyme. The G' and G'' dramatically decreased, indicating the absence of gel state (Figure S11). However, the average molecular weight shows an evident increase by MALDI mass spectrometry, which confirms the crosslinking of the molecules (Figure S12). For further investigation, we performed TEM to characterize the morphology of self-assemblies after the addition of H_2O_2 and HRP. The short fibers with diameter of ~13–25 nm instead of long fibrils are observed, which explicates the absence of the hydrogels (Figure 5). This is because the shorter length of the fibers lacks long range ordering and significantly reduces the physical crosslinking points of the system. In comparison to the long fiber, the larger diameter of short fiber suggests the different arrangement of molecular chains in the micellar cores, possibly due to the chemical cross-linking. The similar gel-to-sol transition was also observed in the other two samples. The short fibers were observed by TEM (Figure S13). As we discussed previously, both hydrophobicity and hydrogen bonding of the PAs result in the formation of long nanofibers. Considering the remained hydrophobicity, it is thus believable that the chemical cross-linking interrupts the hydrogen bonding of PA molecules, particularly the tyrosine −OH groups. This indicates that the phenolic hydroxyl moiety contributes largely to the formation of nanofibers. We further performed DLS to investigate the size of self-assembly in the presence and absence of enzyme. Upon the constant dilution of the solution, it is observed that the size of the self-assembly remains after the addition of enzymes (Figures 6 and S14). In contrast, two distributions of particle size are observed in the solution in the absence of enzyme. The additional size distribution in the range of 2–5 nm suggests the dissociation of the self-assemblies into single molecules. It is thus believable that the physically cross-linked hydrogel transfers into chemically cross-linked nanogel after the addition of H_2O_2 and HRP (Scheme 1).

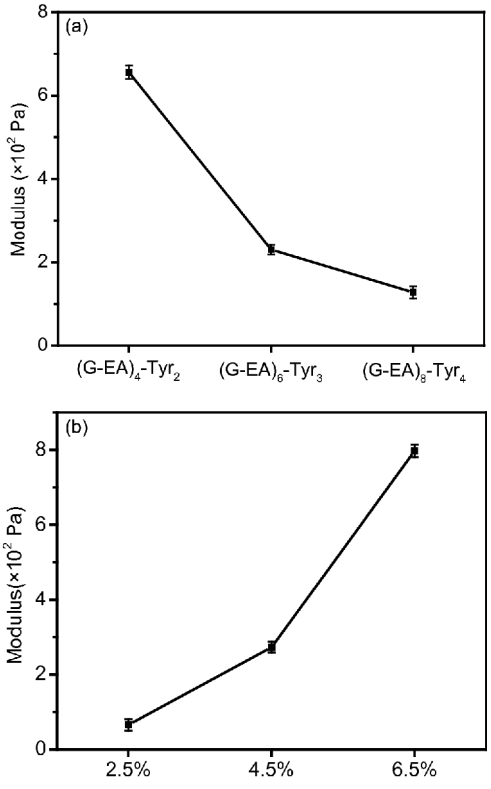

Figure 4 (a) The storage modulus (G') of (G-EA)-*b*-Tyr hydrogel versus strain at a concentration 3.5 wt%. (b) The storage modulus (G') of (G-EA)$_8$-*b*-Tyr$_4$ hydrogel versus strain at different weight concentration.

4 Conclusions

In summary, we have successfully synthesized a novel type

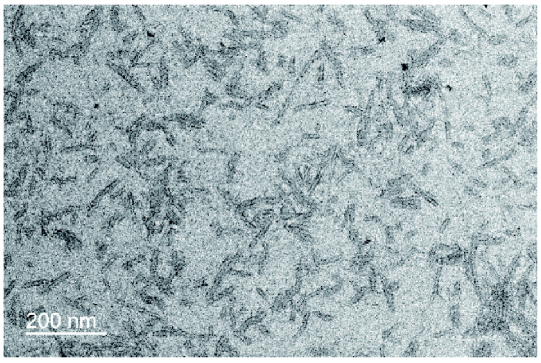

Figure 5 TEM micrograph of sample (G-EA)$_4$-*b*-Tyr$_2$ after enzymatic reaction (1 wt%).

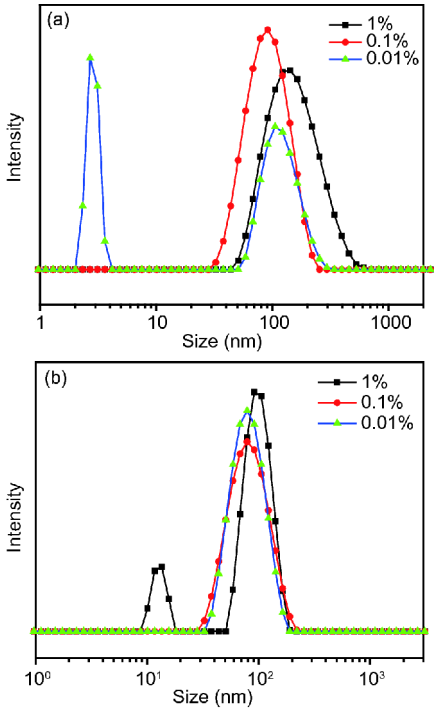

Figure 6 The size distribution of $(G\text{-}EA)_4$-*b*-Tyr_2 (a) before and (b) after enzymatic reaction stimulation at different concentration measured by DLS (color online).

of nonionic peptide amphiphiles by ROP of γ-benzyl-*L*-glutamate *N*-carboxyanhydride (BLG-NCA) and *L*-tyrosine *N*-carboxyanhydride (Tyr-NCA) and subsequent aminolysis. The obtained polymers can readily form a clear hydrogel. The incorporation of tyrosine residues offers hydrophobicity, hydrogen-bonding interaction and enzyme-responsive properties. The effect of DP of the oligomers on the gel properties has been systematically studied. The hydrogel-to-nanogel transition is observed under physiological conditions in the presence of horseradish peroxidase (HRP) and hydrogen peroxide (H_2O_2). We demonstrate that the disruption of hydrogen bonding of phenolic hydroxyl groups leads to the morphology transition, which eventually results in the absence of hydrogel.

Acknowledgements This work was supported by the National Natural Science Foundation of China (21434008, 51503115, 51722302) and Qingdao Innovation Leading Talents Program (3rd).

Conflict of interest The authors declare that they have no conflict of interest.

Supporting information The supporting information is available online at http://chem.scichina.com and http://link.springer.com/journal/11426. The supporting materials are published as submitted, without typesetting or editing. The responsibility for scientific accuracy and content remains entirely with the authors.

1 Bakota EL, Wang Y, Danesh FR, Hartgerink JD. *Biomacromolecules*, 2011, 12: 1651–1657
2 Zhu W, Li Y, Liu L, Chen Y, Wang C, Xi F. *Biomacromolecules*, 2010, 11: 3086–3092
3 Wu EC, Zhang S, Hauser CAE. *Adv Funct Mater*, 2012, 22: 456–468
4 Yan C, Mackay ME, Czymmek K, Nagarkar RP, Schneider JP, Pochan DJ. *Langmuir*, 2012, 28: 6076–6087
5 Scott CM, Forster CL, Kokkoli E. *Langmuir*, 2015, 31: 6122–6129
6 Tsuda Y, Morimoto Y, Takeuchi S. *Langmuir*, 2010, 26: 2645–2649
7 Moyer TJ, Finbloom JA, Chen F, Toft DJ, Cryns VL, Stupp SI. *J Am Chem Soc*, 2014, 136: 14746–14752
8 Niece KL, Czeisler C, Sahni V, Tysseling-Mattiace V, Pashuck ET, Kessler JA, Stupp SI. *Biomaterials*, 2008, 29: 4501–4509
9 Shen Y, Zhang S, Wan Y, Fu W, Li Z. *Soft Matter*, 2015, 11: 2945–2951
10 Lei Y, Rahim M, Ng Q, Segura T. *J Control Release*, 2011, 153: 255–261
11 Nowak AP, Breedveld V, Pakstis L, Ozbas B, Pine DJ, Pochan D, Deming TJ. *Nature*, 2002, 417: 424–428
12 Popescu MT, Liontos G, Avgeropoulos A, Tsitsilianis C. *Soft Matter*, 2015, 11: 331–342
13 Yan Y, de Keizer A, Martens AA, Oliveira CLP, Pedersen JS, de Wolf FA, Drechsler M, Cohen Stuart MA, Besseling NAM. *Langmuir*, 2009, 25: 12899–12908
14 Hartgerink JD, Beniash E, Stupp SI. *Proc Natl Acad Sci USA*, 2002, 99: 5133–5138
15 Jiang H, Guler MO, Stupp SI. *Soft Matter*, 2007, 3: 454–462
16 Cui H, Cheetham AG, Pashuck ET, Stupp SI. *J Am Chem Soc*, 2014, 136: 12461–12468
17 Wan Y, Liu L, Yuan S, Sun J, Li Z. *Langmuir*, 2017, 33: 3234–3240
18 Wan Y, Wang Z, Sun J, Li Z. *Langmuir*, 2016, 32: 7512–7518
19 Meng F, Ni Y, Ji S, Fu X, Wei Y, Sun J, Li Z. *Chin J Polym Sci*, 2017, 35: 1243–1252
20 Fu X, Ma Y, Sun J, Li Z. *Chin J Polym Sci*, 2016, 34: 1436–1447
21 Moriyama K, Minamihata K, Wakabayashi R, Goto M, Kamiya N. *Chem Commun*, 2014, 50: 5895–5898
22 Jin R, Moreira Teixeira LS, Dijkstra PJ, van Blitterswijk CA, Karperien M, Feijen J. *J Control Release*, 2011, 152: 186–195
23 Xu Q, He C, Zhang Z, Ren K, Chen X. *ACS Appl Mater Interfaces*, 2016, 8: 30692–30702
24 Zeng Z, She Y, Peng Z, Wei J, He X. *RSC Adv*, 2016, 6: 8032–8042
25 Ren K, Cui H, Xu Q, He C, Li G, Chen X. *Biomacromolecules*, 2016, 17: 3862–3871
26 Hou J, Li C, Guan Y, Zhang Y, Zhu XX. *Polym Chem*, 2015, 6: 2204–2213
27 Tie ZX, Qin M, Zou DW, Cao Y, Wang W. *Chin Phys Lett*, 2011, 28: 028702
28 Lu YS, Lin YC, Kuo SW. *Macromolecules*, 2012, 45: 6547–6556
29 Huang J, Hastings CL, Duffy GP, Kelly HM, Raeburn J, Adams DJ, Heise A. *Biomacromolecules*, 2013, 14: 200–206
30 Lee Y, Fukushima S, Bae Y, Hiki S, Ishii T, Kataoka K. *J Am Chem Soc*, 2007, 129: 5362–5363
31 Kricheldorf HR, von Lossow C, Schwarz G. *Macromol Chem Phys*, 2004, 205: 918–924
32 Kricheldorf HR, Mutter M, Maser F, Müller D, Förster H. *Biopolymers*, 1983, 22: 1357–1372
33 Paramonov SE, Jun HW, Hartgerink JD. *J Am Chem Soc*, 2006, 128: 7291–7298
34 Ryan DM, Anderson SB, Senguen FT, Youngman RE, Nilsson BL. *Soft Matter*, 2010, 6: 475–479
35 Wang J, Liu K, Yan L, Wang A, Bai S, Yan X. *ACS Nano*, 2016, 10: 2138–2143
36 Lee F, Chung JE, Kurisawa M. *Soft Matter*, 2008, 4: 880–887
37 Kurisawa M, Lee F, Wang LS, Chung JE. *J Mater Chem*, 2010, 20: 5371
38 Ding Y, Li Y, Qin M, Cao Y, Wang W. *Langmuir*, 2013, 29: 13299–13306
39 Li Y, Ding Y, Qin M, Cao Y, Wang W. *Chem Commun*, 2013, 49: 8653–8655